

Closed-Form Expressions for Five-Digit Reflex Camber-Line Design Parameters

Kio M. Lovric*

The University of Sydney, Sydney, NSW 2006, Australia

Despite nearly a century of use in tailless and flying-wing aircraft, the NACA five-digit reflex camber-line family lacks published closed-form expressions for the governing design integrals; practitioners have instead relied on numerical quadrature and tabulated constants available only for a limited set of standard configurations. This paper addresses that gap by deriving closed-form analytical expressions for all lift and zero-moment integrals in terms of elementary functions of the breakpoint and maximum-camber-location parameters. A trigonometric substitution eliminates the endpoint singularities introduced by the Glauert transformation, yielding integrals expressible as inverse trigonometric functions combined with explicit polynomials. The breakpoint parameter is determined by solving a single transcendental equation, and the remaining camber-line constants follow from direct evaluation without numerical integration. Independent verification by numerical quadrature confirms agreement with the analytical expressions to machine precision. Comparison with historical tabulations shows that the closed-form values satisfy the zero-moment design condition to machine precision, whereas substituting the tabulated breakpoints back into the same condition yields residuals nine to thirteen orders of magnitude larger, consistent with the rounding and computational precision available when the original tabulations were produced.

Nomenclature

a_0, a_1, a_2, a_3, a_4	=	polynomial coefficients in forward-region integral derivations
A, B, C_3, C_5, C_7	=	grouped integration coefficients for forward region
A', B', C'_3, C'_5, C'_7	=	grouped integration coefficients for aft region
A_0, A_1, A_2	=	Fourier coefficients of camber-line slope
A_n	=	n th Fourier coefficient of camber-line slope
b_0, b_1, b_2	=	polynomial coefficients in aft-region slope expression
c	=	chord, m

*Undergraduate Researcher, School of Aerospace, Mechanical and Mechatronic Engineering and School of Physics; Student Member AIAA.

c_0, c_1, c_2, c_3, c_4	=	polynomial coefficients in aft-region integral derivations
C_l	=	section lift coefficient
$C_{l,i}$	=	design lift coefficient
$C_{mc/4}$	=	pitching-moment coefficient about quarter-chord
\mathcal{D}	=	denominator polynomial in k_1 expression
dy_c/dx	=	camber-line slope
$I_1^{(l)}, I_2^{(l)}$	=	lift-condition integrals
$I_1^{(m)}, I_2^{(m)}$	=	moment-condition integrals
k_1	=	primary camber-line scaling constant
k_2	=	secondary camber-line scaling constant
L	=	first digit of NACA designation ($C_{l,i} = 0.15L$)
n	=	Fourier series index
P	=	second digit of NACA designation ($x_{mc} = P/20$)
\mathcal{P}	=	polynomial in $I_1^{(m)}$ expression
Q	=	third digit of NACA designation (0 = standard, 1 = reflex)
Q	=	polynomial in $I_2^{(m)}$ expression
r	=	camber-line breakpoint location
\mathcal{R}	=	polynomial in $I_2^{(m)}$ expression
\mathcal{S}	=	polynomial in $I_1^{(l)}$ expression
t	=	airfoil thickness, m
\mathcal{T}	=	polynomial in $I_2^{(l)}$ expression
TT	=	thickness digits ($t/c = TT/100$)
\mathcal{U}	=	polynomial in $I_2^{(l)}$ expression
x	=	chordwise coordinate
x_{mc}	=	maximum camber location
y_c	=	camber-line ordinate

Greek Symbols

α	=	angle of attack, rad
α_i	=	ideal angle of attack, rad
θ	=	Glauert transformation variable, rad
ϕ	=	integration substitution variable, rad

ϕ_r	=	value of ϕ at breakpoint, $\arcsin(\sqrt{r})$, rad
ψ_r	=	complementary angle, $\pi/2 - \phi_r$, rad

Subscripts

anal	=	analytical evaluation
$c/4$	=	quarter-chord
i	=	ideal (design) condition
mc	=	maximum camber
quad	=	numerical quadrature
ref	=	tabulated reference

Superscripts

(l)	=	lift condition
(m)	=	moment condition

I. Introduction

TAILLESS and flying-wing configurations often employ reflexed camber lines to achieve near-zero pitching moment about the quarter-chord, thereby reducing reliance on a horizontal stabilizer for longitudinal trim [1]. Despite decades of use dating to the 1930s [2], determination of the breakpoint location r and the scaling constant k_1 has traditionally relied on numerical evaluation and tabulated values, which exist only for a limited set of standard configurations [3].

In the standard NACA designation *LPQTT*, the first digit L sets the design lift coefficient $C_{l,i} = 0.15 L$, the second digit P locates the maximum camber at $x_{mc} = P/20$, the third digit Q selects the camber-line family ($Q = 0$ for standard, $Q = 1$ for reflex), and the final two digits TT specify the thickness ratio $t/c = TT/100$ [1]. For the reflex family, r is chosen to enforce the zero-moment condition $C_{m_{c/4}} = 0$, and k_1 is then set to satisfy the prescribed design lift coefficient.

While thin-airfoil theory provides closed-form coefficient relations for general camber lines [4], the specific integrals governing the reflex design conditions do not appear to be published in closed form in the standard NACA/NASA tabulations. Here, we derive closed-form expressions for all governing integrals, namely the moment integrals $I_1^{(m)}$ and $I_2^{(m)}$ and the lift integrals $I_1^{(l)}$ and $I_2^{(l)}$, in terms of elementary functions of r and x_{mc} . The resulting expressions eliminate numerical quadrature: r is found by solving $I_1^{(m)} + \frac{1}{(1-r)^3} I_2^{(m)} = 0$ with a single-variable root-finder, and k_1 then follows from direct evaluation.

We validate the analytical results against NASA tabulated values [3] and independent numerical quadrature. The

remainder of this paper is organized as follows: Section II develops the mathematical formulation; Section III presents the closed-form results; Section IV describes the design procedure; Section V presents the validation, and Section VI provides tabled and graphical extended design parameters. Detailed derivations are provided in Appendices A–B.

II. Mathematical Formulation

A. Reflex Camber-Line Geometry

The NACA 5-digit reflex camber line is defined piecewise with maximum camber location parameter $x_{mc} = P/20$, break location r , and scaling constants k_1 and k_2 . The camber-line ordinate is

$$y_c = \begin{cases} \frac{k_1}{6} \left[(x-r)^3 - \frac{k_2}{k_1} (1-r)^3 x - r^3 x + r^3 \right], & 0 \leq x < r \\ \frac{k_1}{6} \left[\frac{k_2}{k_1} (x-r)^3 - \frac{k_2}{k_1} (1-r)^3 x - r^3 x + r^3 \right], & r \leq x \leq 1 \end{cases} \quad (1)$$

The corresponding camber-line slope is

$$\frac{dy_c}{dx} = \begin{cases} \frac{k_1}{6} \left[3(x-r)^2 - \frac{k_2}{k_1} (1-r)^3 - r^3 \right], & 0 \leq x < r \\ \frac{k_1}{6} \left[3 \frac{k_2}{k_1} (x-r)^2 - \frac{k_2}{k_1} (1-r)^3 - r^3 \right], & r \leq x \leq 1 \end{cases} \quad (2)$$

The ratio k_2/k_1 is determined by requiring maximum camber to occur at $x = x_{mc}$, giving

$$\frac{k_2}{k_1} = \frac{3(r - x_{mc})^2 - r^3}{(1-r)^3} \quad (3)$$

Substituting Eq. (3) into Eq. (2) and simplifying yields the working forms of the camber-line slope, written separately for each region. For $0 \leq x < r$,

$$\left(\frac{dy_c}{dx} \right)_{<r} = \frac{k_1}{2} \left(x^2 - 2rx + 2x_{mc}r - x_{mc}^2 \right) \quad (4)$$

and for $r \leq x \leq 1$,

$$\left(\frac{dy_c}{dx} \right)_{\geq r} = \frac{k_1}{2(1-r)^3} \left(b_2 x^2 + b_1 x + b_0 \right) \quad (5)$$

where the polynomial coefficients are

$$b_2 = 3(r - x_{mc})^2 - r^3 \quad (6)$$

$$b_1 = 2r^4 - 6r^3 + 12r^2x_{mc} - 6rx_{mc}^2 \quad (7)$$

$$b_0 = 3r^3 - r^2 - 2r^4x_{mc} - 6r^2x_{mc} + 2rx_{mc} + r^3x_{mc}^2 + 3rx_{mc}^2 - x_{mc}^2 \quad (8)$$

These camber-line slope expressions provide the integrands required by thin-airfoil theory to determine the aerodynamic coefficients.

B. Thin Airfoil Theory

In classical thin-airfoil theory [1, 4], the camber-line slope is expanded in a Fourier cosine series using the Glauert transformation

$$x = \frac{1 - \cos \theta}{2}, \quad \theta \in [0, \pi] \quad (9)$$

The Fourier coefficients are

$$A_0 = \alpha - \frac{1}{\pi} \int_0^\pi \frac{dy_c}{dx} d\theta \quad (10)$$

$$A_n = \frac{2}{\pi} \int_0^\pi \frac{dy_c}{dx} \cos(n\theta) d\theta, \quad n = 1, 2, \dots \quad (11)$$

The section lift and moment coefficients follow as

$$C_l = 2\pi \left(A_0 + \frac{A_1}{2} \right) \quad (12)$$

$$C_{m_{c/4}} = \frac{\pi}{4} (A_2 - A_1) \quad (13)$$

C. Design Constraints

1. Constraint 1: Zero Pitching Moment

For a reflex camber line, the primary design requirement is zero pitching moment about the quarter-chord such that

$$C_{m_{c/4}} = 0 \quad (14)$$

From Eq. (13), this requires $A_2 - A_1 = 0$, which leads to

$$\int_0^\pi \frac{dy_c}{dx} (\cos 2\theta - \cos \theta) d\theta = 0 \quad (15)$$

This constraint is homogeneous in k_1 and determines r (and hence k_2/k_1) by selecting the physically admissible root $r \in (x_{mc}, 1)$; however, since k_1 cancels from the equation, the absolute camber magnitude is not fixed by this condition alone.

2. Constraint 2: Design Lift Coefficient

The ideal angle of attack α_i is defined by $A_0(\alpha_i) = 0$, which eliminates the leading-edge singularity. The design lift coefficient is then

$$C_{l,i} = \pi A_1 = 2 \int_0^\pi \frac{dy_c}{dx} \cos \theta d\theta \quad (16)$$

This constraint, together with the prescribed design lift coefficient, uniquely determines the scaling constant k_1 .

D. Transformation to x -Domain

From the Glauert mapping in Eq. (9), the inverse relations are

$$\cos \theta = 1 - 2x \quad (17)$$

$$\sin \theta = 2\sqrt{x(1-x)} \quad (18)$$

For the moment condition,

$$\cos 2\theta - \cos \theta = (2 \cos^2 \theta - 1) - \cos \theta = 8x^2 - 6x \quad (19)$$

while for the lift condition, $\cos \theta = 1 - 2x$ follows directly from Eq. (17). The Jacobian associated with the mapping is

$$d\theta = \frac{dx}{\sqrt{x(1-x)}} \quad (20)$$

so that $\theta \in [0, \pi]$ corresponds to $x \in [0, 1]$.

E. Formulation of the Design Integrals

Both design constraints reduce to weighted integrals over $x \in [0, 1]$ with the common Jacobian $dx/\sqrt{x(1-x)}$ arising from the Glauert mapping. Because the reflex camber-line slope is piecewise-defined with a breakpoint at $x = r$, each constraint naturally splits into a forward contribution ($0 \leq x < r$) and an aft contribution ($r \leq x \leq 1$). The resulting integrals share the same integrable endpoint singularities associated with $1/\sqrt{x(1-x)}$; these are removed in the closed-form evaluation by the substitution $x = \sin^2 \phi$ (see Section II.F).

1. Moment Condition Integrals

Substituting Eq. (20) into Eq. (15) and using Eq. (19), the zero-moment condition becomes

$$\int_0^1 \frac{dy_c}{dx} \frac{8x^2 - 6x}{\sqrt{x(1-x)}} dx = 0 \quad (21)$$

Splitting at $x = r$ and substituting the simplified slope expressions Eqs. (4) and (5) yields

$$\frac{k_1}{2} \left[I_1^{(m)} + \frac{1}{(1-r)^3} I_2^{(m)} \right] = 0 \quad (22)$$

where the reduced moment integrals, independent of k_1 , are defined as

$$I_1^{(m)} \equiv \int_0^r \left(x^2 - 2rx + 2x_{mc}r - x_{mc}^2 \right) \frac{8x^2 - 6x}{\sqrt{x(1-x)}} dx \quad (23)$$

$$I_2^{(m)} \equiv \int_r^1 \left(b_2 x^2 + b_1 x + b_0 \right) \frac{8x^2 - 6x}{\sqrt{x(1-x)}} dx \quad (24)$$

Since $k_1 \neq 0$ for a nontrivial camber line, it may be divided out, and the breakpoint parameter r is determined by

$$I_1^{(m)} + \frac{1}{(1-r)^3} I_2^{(m)} = 0 \quad (25)$$

2. Lift Condition Integrals

The lift constraint follows in the same manner, with $\cos \theta = 1 - 2x$. Substituting Eq. (20) into Eq. (16) gives

$$C_{l,i} = 2 \int_0^1 \frac{dy_c}{dx} \frac{1 - 2x}{\sqrt{x(1-x)}} dx \quad (26)$$

Splitting at $x = r$ and substituting Eqs. (4) and (5) yields

$$C_{l,i} = k_1 \left[I_1^{(l)} + \frac{1}{(1-r)^3} I_2^{(l)} \right] \quad (27)$$

where

$$I_1^{(l)} \equiv \int_0^r \left(x^2 - 2rx + 2x_{mc}r - x_{mc}^2 \right) \frac{1 - 2x}{\sqrt{x(1-x)}} dx \quad (28)$$

$$I_2^{(l)} \equiv \int_r^1 \left(b_2 x^2 + b_1 x + b_0 \right) \frac{1 - 2x}{\sqrt{x(1-x)}} dx \quad (29)$$

The prescribed design lift coefficient $C_{l,i} = 0.15L$ then determines the scaling constant

$$k_1 = \frac{C_{l,i}}{I_1^{(l)} + \frac{1}{(1-r)^3} I_2^{(l)}} \quad (30)$$

F. Trigonometric Substitution

The design integrals in Eqs. (23)–(29) contain the Glauert Jacobian $1/\sqrt{x(1-x)}$, which produces integrable algebraic endpoint singularities at $x = 0$ and $x = 1$ (typically $\sim x^{-1/2}$ as $x \rightarrow 0$ and $\sim (1-x)^{-1/2}$ as $x \rightarrow 1$, up to the polynomial numerators). Although the integrals converge, these square-root factors obscure direct antiderivative evaluation in the x -domain. A standard remedy is to introduce an angle variable for which the Jacobian cancels identically.

Accordingly, we apply the substitution

$$x = \sin^2 \phi, \quad dx = 2 \sin \phi \cos \phi d\phi, \quad \sqrt{x(1-x)} = \sin \phi \cos \phi \quad (31)$$

so that the weighted measure simplifies to a constant,

$$\frac{dx}{\sqrt{x(1-x)}} = 2 d\phi \quad (32)$$

Under this mapping, the integrands become polynomial combinations of $\sin^{2n} \phi$ (and, where required, $\cos^{2n} \phi$) with constant measure $d\phi$, enabling closed-form evaluation via standard trigonometric antiderivatives. The limits map as

$$x = 0 \Rightarrow \phi = 0, \quad x = r \Rightarrow \phi = \phi_r \equiv \arcsin(\sqrt{r}), \quad x = 1 \Rightarrow \phi = \frac{\pi}{2} \quad (33)$$

It is often convenient to note the complementary relation $\arccos(\sqrt{r}) = \frac{\pi}{2} - \phi_r$ for the aft-region expressions.

III. Closed-Form Results

For clarity, we present the closed-form *definite* expressions first; full derivations appear in Appendices A–B.

A. Moment Condition Integrals

1. *Integral $I_1^{(m)}$ over $0 \leq x < r$*

$$I_1^{(m)} = \frac{5 - 8r}{8} \arcsin(\sqrt{r}) + \sqrt{r(1-r)} \mathcal{P}(r, x_{mc}) \quad (34)$$

where

$$\mathcal{P}(r, x_{mc}) = 4r(x_{mc} - r)^2 + \frac{-16r^3 + 8r^2 + 14r - 15}{24} \quad (35)$$

2. Integral $I_2^{(m)}$ over $r \leq x \leq 1$

$$I_2^{(m)} = Q(r, x_{mc}) \arccos(\sqrt{r}) - \sqrt{r(1-r)} \mathcal{R}(r, x_{mc}) \quad (36)$$

where

$$Q(r, x_{mc}) = \frac{8r-5}{8} \left[r^3 - 3(x_{mc} - r)^2 \right] \quad (37)$$

and

$$\mathcal{R}(r, x_{mc}) = \frac{r^3}{24} (16r^3 - 8r^2 - 14r + 15) - \frac{1}{8} (32r^4 - 80r^3 + 88r^2 - 46r + 15) (x_{mc} - r)^2 \quad (38)$$

B. Lift Condition Integrals

1. Integral $I_1^{(l)}$ over $0 \leq x < r$

$$I_1^{(l)} = \left(r - \frac{1}{2} \right) \arcsin(\sqrt{r}) + \sqrt{r(1-r)} \mathcal{S}(r, x_{mc}) \quad (39)$$

where

$$\mathcal{S}(r, x_{mc}) = \frac{1}{3} + \frac{2}{3} \left(r - \frac{1}{2} \right)^2 - 2(x_{mc} - r)^2 \quad (40)$$

2. Integral $I_2^{(l)}$ over $r \leq x \leq 1$

$$I_2^{(l)} = \mathcal{T}(r, x_{mc}) \arccos(\sqrt{r}) - \sqrt{r(1-r)} \mathcal{U}(r, x_{mc}) \quad (41)$$

where

$$\mathcal{T}(r, x_{mc}) = \left(\frac{1}{2} - r \right) \left[r^3 - 3(x_{mc} - r)^2 \right] \quad (42)$$

and

$$\mathcal{U}(r, x_{mc}) = \frac{1}{2} (4r^3 - 8r^2 + 8r - 1) (x_{mc} - r)^2 - \frac{r^3}{6} (4r^2 - 4r + 3) \quad (43)$$

IV. Design Procedure

A. Solution for Breakpoint Parameter r

The zero-pitching-moment condition requires $I_1^{(m)} + \frac{1}{(1-r)^3} I_2^{(m)} = 0$. Substituting the closed-form expressions yields a transcendental equation in r and x_{mc} only:

$$\begin{aligned} & \frac{5-8r}{8} \arcsin(\sqrt{r}) + \sqrt{r(1-r)} \mathcal{P}(r, x_{mc}) \\ & + \frac{Q(r, x_{mc}) \arccos(\sqrt{r}) - \sqrt{r(1-r)} \mathcal{R}(r, x_{mc})}{(1-r)^3} = 0 \end{aligned} \quad (44)$$

This equation is solved numerically for r given x_{mc} , but crucially, no numerical integration is required; all terms are evaluated in closed form. When multiple roots exist in $(0, 1)$, the breakpoint must satisfy $r > x_{mc}$ so that maximum camber occurs forward of the reflex region; the smallest such root is selected. For the standard range $P \in [1, 5]$, the transcendental equation admits a unique root in $(x_{mc}, 1)$, and the left-hand side of Eq. (44) is monotonic in this interval, ensuring robust convergence for standard root-finding algorithms (see Fig. 1, lower-right panel). Equivalently, the function $f(r; x_{mc}) := I_1^{(m)} + (1-r)^{-3} I_2^{(m)}$ has exactly one zero on $(x_{mc}, 1)$ for $P \in [1, 5]$, so bracketing in this interval guarantees convergence. As P increases beyond 5, the root approaches unity and the reflex curvature becomes impractically large; for $P = 9$, Eq. (44) admits no admissible root $r \in (x_{mc}, 1)$. Physically, the breakpoint r represents the chordwise location where the camber-line curvature changes sign; moving maximum camber forward (decreasing x_{mc}) requires a correspondingly forward breakpoint to maintain the moment balance needed for zero pitching moment.

B. Solution for Scaling Constant k_1

Once r is determined, the scaling constant k_1 follows directly from Eq. (30). Substituting the closed-form expressions (39)–(41):

$$k_1 = \frac{C_{l,i}}{\mathcal{D}(r, x_{mc})} \quad (45)$$

where the denominator is

$$\begin{aligned} \mathcal{D}(r, x_{mc}) &= \left(r - \frac{1}{2}\right) \arcsin(\sqrt{r}) + \sqrt{r(1-r)} \mathcal{S}(r, x_{mc}) \\ &+ \frac{1}{(1-r)^3} \left[\mathcal{T}(r, x_{mc}) \arccos(\sqrt{r}) - \sqrt{r(1-r)} \mathcal{U}(r, x_{mc})\right] \end{aligned} \quad (46)$$

C. Complete Design Algorithm

The preceding results can be assembled into a straightforward procedure for computing the camber-line parameters directly from a NACA designation. Given a NACA *LPQTT* designation with $Q = 1$ (reflex):

- 1) *Input:* Extract L and P from the designation. Compute $x_{mc} = P/20$ and $C_{l,i} = 0.15L$.

- 2) *Solve for r :* Find the root of Eq. (44) in the interval $(x_{mc}, 1)$ using a one-dimensional root-finding algorithm (e.g., bisection, secant, Newton–Raphson, Brent’s method, or regula falsi).
- 3) *Compute k_2/k_1 :* Evaluate Eq. (3).
- 4) *Compute k_1 :* Evaluate Eq. (45) with the known values of r , x_{mc} , and $C_{l,i}$.
- 5) *Compute k_2 :* $k_2 = (k_2/k_1) \cdot k_1$.
- 6) *Output:* Complete camber-line parameters (r, k_1, k_2) .

All steps involve only closed-form evaluations and a single root-finding operation; no numerical quadrature is required. When r approaches x_{mc} , the ratio k_2/k_1 becomes sensitive to rounding, so double-precision arithmetic is recommended throughout. The expressions involving $\arcsin(\sqrt{r})$ and $\arccos(\sqrt{r})$ are numerically well-conditioned for all $r \in (0, 1)$, and no cancellation issues arise in the polynomial terms.

V. Validation and Discussion

The closed-form expressions derived in the preceding sections were validated against tabulated reference values for the NACA 5-digit reflex camber-line series as compiled by Ladson and Brooks [3]. The analytically computed breakpoint parameter r and scaling constants k_1 and k_2/k_1 are compared with tabulated values, and the moment and lift integrals are independently verified by numerical quadrature of the original definitions. A sensitivity analysis is then performed to determine whether observed discrepancies arise from the propagation of small differences in r or from other sources. Graphical comparisons supplement the tabulated results.

A. Validation of Breakpoint Parameter r

The design parameter r was obtained by solving the design constraint

$$I_1^{(m)}(r; x_{mc}) + \frac{1}{(1-r)^3} I_2^{(m)}(r; x_{mc}) = 0 \quad (47)$$

The root was computed using MATLAB’s `fzero`, with $I_1^{(m)}$ and $I_2^{(m)}$ evaluated analytically using the derived closed forms. Table 2 compares the resulting values with the tabulations [3].

Table 2 Closed-form breakpoint parameter r compared with tabulated values [3].

Designation	x_{mc}	r_{ref}	r_{anal}	$r_{\text{anal}} - r_{\text{ref}}$	$\left \left(I_1^{(m)} + \frac{1}{(1-r)^3} I_2^{(m)} \right)_{\text{anal}} \right $
221	0.10	0.1300	0.1307	$+7.50 \times 10^{-4}$	3.59×10^{-17}
231	0.15	0.2170	0.2160	-9.85×10^{-4}	2.78×10^{-15}
241	0.20	0.3180	0.3179	-8.10×10^{-5}	1.09×10^{-15}
251	0.25	0.4410	0.4408	-1.70×10^{-4}	3.99×10^{-17}

The maximum absolute discrepancy is 9.85×10^{-4} , with a mean of 4.97×10^{-4} . The residuals $\left| \left(I_1^{(m)} + \frac{1}{(1-r)^3} I_2^{(m)} \right)_{\text{anal}} \right|$

at the analytical solutions are 10^{-15} – 10^{-17} , indicating near machine-precision satisfaction of the design constraint. For reproducibility, the computed values to eight decimal places are provided in Appendix C.

B. Independent Quadrature Verification of Moment Integrals

To independently verify the analytical expressions for $I_1^{(m)}$ and $I_2^{(m)}$, we evaluate the original integral definitions by numerical quadrature at the same (x_{mc}, r) pairs and compare against the corresponding analytical values. Applying the same trigonometric substitution introduced in Section II.F, $I_1^{(m)}$ and $I_2^{(m)}$ are evaluated by quadrature on $\phi \in [0, \phi_r]$ and $\phi \in [\phi_r, \pi/2]$, respectively, with smooth ϕ -space integrands. Table 3 confirms agreement between analytical and quadrature evaluations at the level of 10^{-17} – 10^{-18} , providing stringent end-to-end verification of the moment integral derivations.

Table 3 Independent quadrature verification of moment integrals.

Case	x_{mc}	r	$ I_{1,\text{anal}}^{(m)} - I_{1,\text{quad}}^{(m)} $	$ I_{2,\text{anal}}^{(m)} - I_{2,\text{quad}}^{(m)} $	$ (I_1^{(m)} + \frac{1}{(1-r)^3} I_2^{(m)})_{\text{quad}} $
221	0.10	0.13074976	2.17×10^{-17}	2.44×10^{-18}	1.04×10^{-17}
231	0.15	0.21601450	3.51×10^{-17}	4.34×10^{-19}	2.81×10^{-15}
241	0.20	0.31791890	3.82×10^{-17}	3.04×10^{-18}	1.05×10^{-15}
251	0.25	0.44083034	1.56×10^{-17}	2.43×10^{-17}	8.33×10^{-17}

C. Independent Quadrature Verification of Lift Integrals

The same verification procedure was applied to the lift integrals $I_1^{(l)}$ and $I_2^{(l)}$. Table 4 confirms agreement between analytical and quadrature evaluations at the level of 10^{-17} – 10^{-18} , providing complete verification of the lift integral derivations.

Table 4 Independent quadrature verification of lift integrals.

Case	x_{mc}	r	$ I_{1,\text{anal}}^{(l)} - I_{1,\text{quad}}^{(l)} $	$ I_{2,\text{anal}}^{(l)} - I_{2,\text{quad}}^{(l)} $
221	0.10	0.13074976	6.07×10^{-18}	2.30×10^{-18}
231	0.15	0.21601450	2.78×10^{-17}	4.55×10^{-18}
241	0.20	0.31791890	1.39×10^{-17}	4.34×10^{-18}
251	0.25	0.44083034	0	1.60×10^{-17}

D. Validation of Scaling Constant k_1

The scaling constant k_1 was computed using Eq. (45) with the analytically determined r values and compared against the tabulated reference values [3]. Table 5 presents the results.

Across these cases, k_1 is reproduced to within 1.7% of the tabulations. The largest discrepancies occur for the 221 and 231 cases, where k_1 is large because the effective camber is small when $r \approx x_{mc}$. However, as demonstrated in Section V.F, these discrepancies cannot be attributed to the propagation of errors in r . A first-order sensitivity

Table 5 Comparison of computed k_1 values against tabulations [3].

Designation	x_{mc}	L	$(k_1)_{\text{ref}}$	$(k_1)_{\text{anal}}$	Absolute Error	Relative Error
221	0.10	2	51.990	51.120	0.870	1.67%
231	0.15	2	15.793	15.691	0.102	0.65%
241	0.20	2	6.520	6.507	0.013	0.19%
251	0.25	2	3.191	3.176	0.015	0.48%

analysis predicts that the $\mathcal{O}(10^{-3})$ differences in r would produce changes in k_1 of only $\mathcal{O}(10^{-2})$, whereas the observed discrepancies are $\mathcal{O}(10^{-1})$ to $\mathcal{O}(1)$.

The discrepancies, therefore, reflect differences in the original tabulation methodology rather than errors in the present derivation. Possible sources include different numerical quadrature schemes or limited floating-point precision in the legacy NACA-era computations, rounding of intermediate parameters before computing k_1 , or minor differences in conventions or governing equations. Crucially, the closed-form lift integrals underlying Eq. (45) are independently verified against numerical quadrature to machine precision (Section V.C), confirming the analytical correctness of the present expressions. The closed-form k_1 values may therefore represent a more accurate evaluation than the legacy tabulations.

E. Verification of k_2/k_1 Ratio

As a supplementary check, the ratio k_2/k_1 was computed using Eq. (3) with the analytically determined r values and then compared against the tabulated reference values [3]. Table 6 presents the results. Although the relative errors for the 221 and 231 cases appear large (up to 20%), this is a consequence of the small magnitude of k_2/k_1 rather than a deficiency in the analytical expressions. As confirmed by the sensitivity analysis in Section V.F, these discrepancies are fully explained by the propagation of $\mathcal{O}(10^{-3})$ differences in r : the discrepancies estimated from $\frac{\partial(k_2/k_1)}{\partial r} \cdot \Delta r$ match the observed values to within $\approx 10\%$ (Table 7).

Table 6 Verification of k_2/k_1 ratio against tabulations [3].

Designation	$(k_2/k_1)_{\text{ref}}$	$(k_2/k_1)_{\text{anal}}$	Absolute Error	Relative Error
221	0.000764	0.000916	1.52×10^{-4}	19.85%
231	0.006770	0.006213	5.57×10^{-4}	8.22%
241	0.030300	0.030195	1.05×10^{-4}	0.35%
251	0.135500	0.134878	6.22×10^{-4}	0.46%

From Eq. (3), the ratio k_2/k_1 depends on the numerator $3(r - x_{mc})^2 - r^3$, which approaches zero as $r \rightarrow x_{mc}$. Physically, a small k_2/k_1 indicates minimal reflex in the aft region, and in this limit the camber line is nearly cubic throughout; the ratio therefore becomes ill-conditioned with respect to r . For the 221 case, $(r - x_{mc}) \approx 0.03$ and the numerator is $\mathcal{O}(10^{-3})$. A discrepancy of $\mathcal{O}(10^{-4})$ in r thus propagates to a comparable absolute error in k_2/k_1 , but

represents a large fraction of the small ratio. For the 241 and 251 cases, the breakpoint lies further aft, $(r - x_{mc})$ is larger, and k_2/k_1 is correspondingly of order 10^{-2} to 10^{-1} ; the same absolute errors in r now produce relative errors below 0.5%. This confirms that the analytical expression is accurate and that the apparent discrepancies for forward-camber cases are a quantitatively predictable consequence of parametric sensitivity rather than analytical error.

F. Sensitivity Analysis

The discrepancies observed in Sections V.D and V.E can be examined through a sensitivity analysis measuring how small perturbations in r propagate into k_2/k_1 and k_1 .

1. Sensitivity of k_2/k_1

From Eq. (3), the derivative of k_2/k_1 with respect to r is obtained via the quotient rule:

$$\frac{\partial}{\partial r} \left(\frac{k_2}{k_1} \right) = \frac{[6(r - x_{mc}) - 3r^2] (1 - r)^3 + 3(1 - r)^2 [3(r - x_{mc})^2 - r^3]}{(1 - r)^6} \quad (48)$$

Table 7 presents the computed sensitivities and demonstrates that the observed discrepancies are well-predicted by the first-order approximation $\Delta(k_2/k_1)_{\text{anal}} \approx \frac{\partial(k_2/k_1)}{\partial r} \cdot \Delta r$. The close agreement between analytical and reference

Table 7 Sensitivity analysis for k_2/k_1 : comparison of analytical and reference discrepancies.

Designation	r	$\frac{\partial(k_2/k_1)}{\partial r}$	Δr	$\Delta(k_2/k_1)_{\text{anal}}$	$\Delta(k_2/k_1)_{\text{ref}}$
221	0.1307	0.206	$+7.50 \times 10^{-4}$	$+1.54 \times 10^{-4}$	$+1.52 \times 10^{-4}$
231	0.2160	0.555	-9.85×10^{-4}	-5.47×10^{-4}	-5.57×10^{-4}
241	0.3179	1.407	-8.10×10^{-5}	-1.14×10^{-4}	-1.05×10^{-4}
251	0.4408	3.938	-1.70×10^{-4}	-6.68×10^{-4}	-6.22×10^{-4}

discrepancies confirms that the k_2/k_1 differences arise entirely from the propagation of small errors in r . For the 221 case, $\partial(k_2/k_1)/\partial r \approx 0.21$. Although this sensitivity is modest, the ratio $k_2/k_1 \approx 0.0009$ is itself small, so even minor absolute changes appear as large relative errors. The sensitivity increases as the breakpoint moves aft, reaching $\partial(k_2/k_1)/\partial r \approx 3.9$ for the 251 case. Yet, the larger baseline value of $k_2/k_1 \approx 0.135$ renders these variations less significant in relative terms.

2. Sensitivity of k_1

The sensitivity of k_1 to perturbations in r is computed numerically from Eq. (45). Table 8 presents the results. Unlike k_2/k_1 , the analytical discrepancies in k_1 from error propagation in r do not explain the reference differences. For example, in the 221 case, the sensitivity $\partial k_1/\partial r \approx -13.5$ with $\Delta r \approx 7.5 \times 10^{-4}$ predicts $\Delta k_1 \approx -0.01$. However, the reference discrepancy is -0.87 , nearly two orders of magnitude larger. This indicates that the k_1 discrepancies arise primarily from differences in how the original tabulations were computed, rather than propagation of r errors alone.

Table 8 Sensitivity analysis for k_1 : comparison of analytical and reference discrepancies.

Designation	r	$\frac{\partial k_1}{\partial r}$	Δr	$\Delta k_{1,\text{anal}}$	$\Delta k_{1,\text{ref}}$
221	0.1307	-13.5	$+7.50 \times 10^{-4}$	-0.010	-0.870
231	0.2160	+1.70	-9.85×10^{-4}	-0.002	-0.102
241	0.3179	+2.52	-8.10×10^{-5}	-0.000	-0.013
251	0.4408	+2.15	-1.70×10^{-4}	-0.000	-0.015

Possible sources include different numerical quadrature schemes or precision in legacy computations, intermediate value rounding before computing k_1 , or slight differences in the governing equations or conventions used historically.

G. Graphical Validation

Fig. 1 provides a visual summary of the agreement between the analytical $r(x_{mc})$ relation and the reference values [3]. The left panel displays the analytical mapping of r versus x_{mc} (solid line), along with the reference points and analytical roots, which are visually coincident. The dashed line $r = x_{mc}$ indicates the boundary of the physically admissible region $r > x_{mc}$. The upper-right panel plots the signed discrepancy scaled by 10^4 , confirming deviations of order 10^{-3} , while the lower-right panel shows $I_1^{(m)} + \frac{1}{(1-r)^3} I_2^{(m)}$ as a function of r for each x_{mc} , demonstrating clear zero-crossings at the solution values.

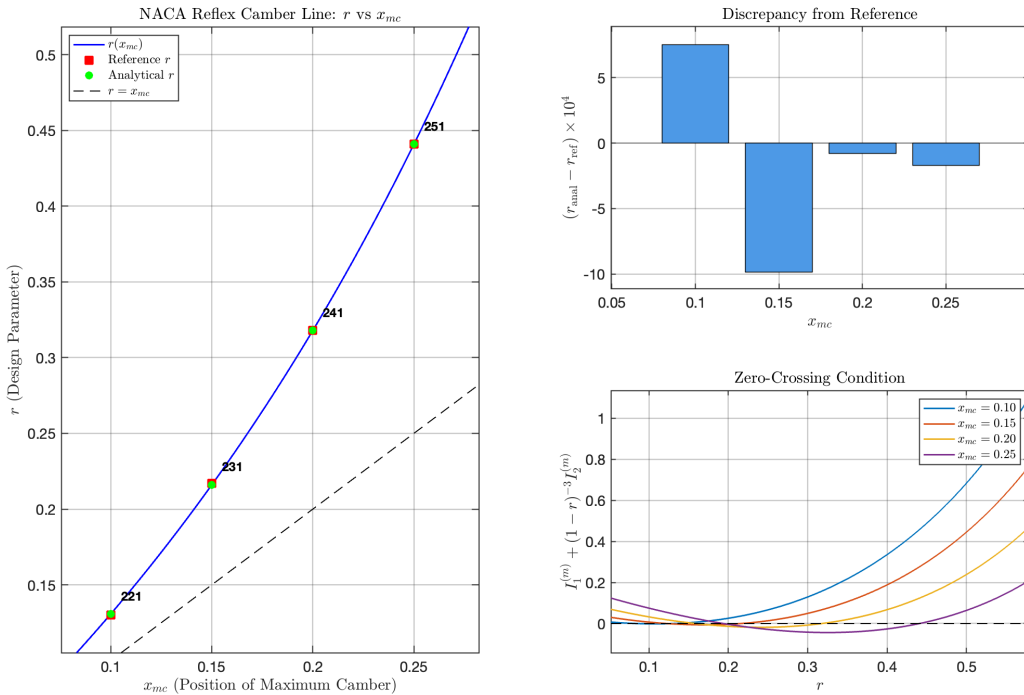


Fig. 1 Validation of breakpoint parameter r : (left) analytical and reference [3] values versus x_{mc} ; (upper right) discrepancy $r_{\text{anal}} - r_{\text{ref}}$; (lower right) moment-condition residual versus r .

Fig. 2 presents corresponding results for the scaling constant k_1 . The left panel shows the analytical $k_1(x_{mc})$ relation, which exhibits the expected asymptotic increase as x_{mc} decreases (requiring larger k_1 to achieve the design lift when the effective camber is reduced). The upper-right panel displays the signed discrepancy $k_{1,\text{anal}} - k_{1,\text{ref}}$, showing the largest deviation for the 221 case. The lower-right panel verifies that the design lift coefficient $C_{l,i} = 0.3$ (corresponding to $L = 2$) is correctly recovered across all cases, confirming internal consistency of the closed-form lift-integral formulation.

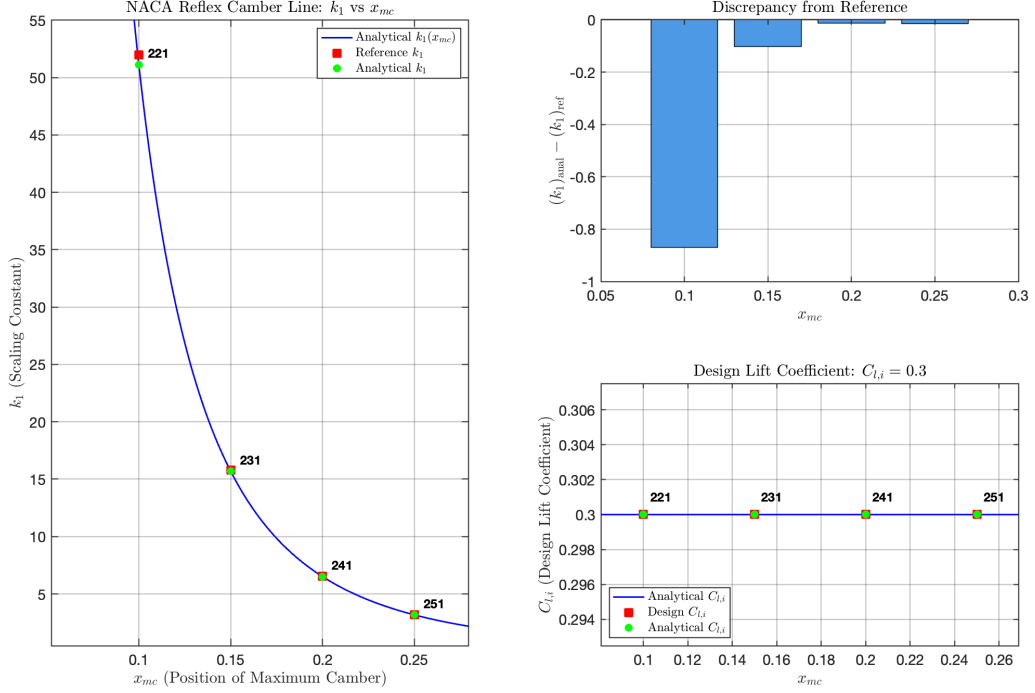


Fig. 2 Validation of scaling constant k_1 : (left) analytical and reference [3] values versus x_{mc} ; (upper right) discrepancy $k_{1,\text{anal}} - k_{1,\text{ref}}$; (lower right) recovered $C_{l,i}$.

H. Discussion

The validation results demonstrate that the closed-form analytical framework reproduces the reference design parameters [3] to within $O(10^{-3})$ for r and $O(10^{-2})$ for k_1 across the representative cases 221, 231, 241, and 251. Table 9 summarises the principal validation metrics, and the sensitivity analysis (Section V.F) clarifies the origin and significance of the observed discrepancies.

The analytical values of the breakpoint parameter r satisfy the zero-moment condition to machine precision (10^{-15} – 10^{-17}), and agree with the reference tabulations to within the expected rounding uncertainty associated with four-decimal-place reporting. In this sense, the closed-form moment framework should be interpreted as providing higher-precision breakpoint locations consistent with the original condition, rather than merely reproducing rounded

Table 9 Summary of validation metrics (cases: 221, 231, 241, 251).

Metric	Value
Maximum $ r_{\text{anal}} - r_{\text{ref}} $	9.85×10^{-4}
Mean $ r_{\text{anal}} - r_{\text{ref}} $	4.97×10^{-4}
Maximum moment-condition residual $ I_1^{(m)} + \frac{1}{(1-r)^3} I_2^{(m)} $	2.78×10^{-15}
Maximum $ k_{1,\text{anal}} - k_{1,\text{ref}} $	0.87
Maximum relative error in k_1	1.67%
Maximum $ (k_2/k_1)_{\text{anal}} - (k_2/k_1)_{\text{ref}} $	6.22×10^{-4}

reference values.

The discrepancies in the ratio k_2/k_1 between analytical and reference values are quantitatively explained by the propagation of $\mathcal{O}(10^{-3})$ differences in r through the sensitivity $\partial(k_2/k_1)/\partial r$. This behaviour is consistent with the first-order estimate

$$\Delta\left(\frac{k_2}{k_1}\right) \approx \frac{\partial(k_2/k_1)}{\partial r} \Delta r \quad (49)$$

and confirms that the closed-form expression for k_2/k_1 is verified. Practically, this implies that the reference scatter in k_2/k_1 is an expected consequence of rounding in r , rather than an inconsistency in the present formulation.

In contrast, the observed discrepancies in the scaling constant k_1 are not explained by r error propagation: the analytical perturbations based on $\partial k_1/\partial r$ are $\mathcal{O}(10^{-2})$, while the reference differences are $\mathcal{O}(10^{-1})$ to $\mathcal{O}(1)$ for the cases considered. Given that the lift-condition integrals are independently verified by numerical quadrature to machine precision (Table 4), the most plausible explanation is that the reference k_1 values reflect differences in legacy computational methodology, such as historical quadrature, intermediate rounding or implementation conventions, rather than deficiencies in the present closed-form derivation.

The sensitivity results further show that when $r \approx x_{mc}$, a regime characteristic of forward-camber reflex configurations, both k_2/k_1 and k_1 become more sensitive to the breakpoint location. In this regime, small perturbations in r can induce disproportionately large changes in the derived constants, thus underscoring the value of computing r to higher precision from the exact zero-moment condition rather than relying on four-decimal-place tabulations.

Finally, the analytical expressions are corroborated independently by direct numerical quadrature of the original integral definitions, yielding agreement at the level of 10^{-17} – 10^{-18} for the moment integrals (Table 3) and 10^{-17} – 10^{-18} for the lift integrals (Table 4). This provides stringent verification of the closed-form results and supports the use of the present framework as a higher-precision alternative to reference tabulations.

VI. Extended Design Parameters

The closed-form expressions enable computation of design parameters for any valid NACA 5-digit reflex designation. Table 10 presents values for the standard ranges $P \in [1, 5]$ and $L \in [1, 6]$, corresponding to $x_{mc} \in [0.05, 0.25]$ and

$C_{l,i} \in [0.15, 0.90]$. Beyond $P = 5$, the ratio k_2/k_1 increases rapidly, indicating impractically large reflex curvature. Consistently, for $P = 9$ Eq. (44) admits no admissible root $r \in (x_{mc}, 1)$. The tabulated values of r and k_2/k_1 depend only on x_{mc} and are therefore constant within each group of fixed P , while k_1 and k_2 scale linearly with the design lift coefficient; the latter is computed simply as $k_2 = (k_2/k_1) \cdot k_1$.

Table 10 Design parameters for NACA 5-digit reflex camber lines.

Camber-line					
designation	x_{mc}	r	k_1	k_2/k_1	k_2
111	0.05	0.0591	174.582	0.000051	0.008904
121	0.10	0.1307	25.560	0.000916	0.023413
131	0.15	0.2160	7.845	0.006213	0.048742
141	0.20	0.3179	3.254	0.030195	0.098255
151	0.25	0.4408	1.588	0.134878	0.214186
211	0.05	0.0591	349.163	0.000051	0.017807
221	0.10	0.1307	51.120	0.000916	0.046826
231	0.15	0.2160	15.691	0.006213	0.097488
241	0.20	0.3179	6.507	0.030195	0.196496
251	0.25	0.4408	3.176	0.134878	0.428332
311	0.05	0.0591	523.745	0.000051	0.026711
321	0.10	0.1307	76.680	0.000916	0.070239
331	0.15	0.2160	23.536	0.006213	0.146230
341	0.20	0.3179	9.761	0.030195	0.294751
351	0.25	0.4408	4.763	0.134878	0.642439
411	0.05	0.0591	698.327	0.000051	0.035615
421	0.10	0.1307	102.240	0.000916	0.093652
431	0.15	0.2160	31.382	0.006213	0.194976
441	0.20	0.3179	13.015	0.030195	0.392993
451	0.25	0.4408	6.351	0.134878	0.856624
511	0.05	0.0591	872.908	0.000051	0.044518
521	0.10	0.1307	127.801	0.000916	0.117066
531	0.15	0.2160	39.227	0.006213	0.243718
541	0.20	0.3179	16.268	0.030195	0.491234
551	0.25	0.4408	7.939	0.134878	1.070810
611	0.05	0.0591	1047.490	0.000051	0.053422
621	0.10	0.1307	153.361	0.000916	0.140479
631	0.15	0.2160	47.073	0.006213	0.292464
641	0.20	0.3179	19.522	0.030195	0.589489
651	0.25	0.4408	9.527	0.134878	1.284996

VII. Conclusion

Closed-form analytical expressions have been derived for all thin-airfoil integrals arising in the design of NACA 5-digit reflex camber lines. The moment integrals $I_1^{(m)}$ and $I_2^{(m)}$ admit closed-form representations involving $\arcsin(\sqrt{r})$, $\arccos(\sqrt{r})$, and polynomial contributions \mathcal{P} , \mathcal{Q} , \mathcal{R} in r and x_{mc} , while the lift integrals $I_1^{(l)}$ and $I_2^{(l)}$ admit analogous representations with polynomial contributions \mathcal{S} , \mathcal{T} , \mathcal{U} . The breakpoint parameter r is obtained by solving the transcendental condition $I_1^{(m)} + \frac{1}{(1-r)^3} I_2^{(m)} = 0$ using one-dimensional root-finding, thus requiring no numerical integration; the resulting values satisfy the zero-moment condition to machine precision and provide higher-precision breakpoint locations than four-decimal-place legacy tabulations. The scaling constant k_1 follows from direct closed-form evaluation, rendering the complete design workflow quadrature-free. The observed differences in k_2/k_1 relative to legacy tabulations are explained quantitatively by propagation of rounding errors in r , constituting indirect verification of the closed-form expressions; in regimes where $r \approx x_{mc}$, the elevated sensitivity of both k_2/k_1 and k_1 makes the higher-precision r values particularly valuable.

The resulting formulation replaces repeated numerical quadrature with analytically evaluable expressions, therefore improving reproducibility and computational efficiency. By eliminating numerical integration from the design process, the present work removes a source of variability that has persisted in the literature for nearly a century. Independent quadrature verification of both moment and lift integrals to machine precision confirms the analytical correctness of the present expressions, which may therefore represent a more accurate evaluation than legacy tabulations. The extended parameter tables provided herein offer a comprehensive reference for designations beyond the limited set available in historical NACA tabulations. The methodology presented here may be extended to other piecewise-defined camber-line families or adapted for use in automated airfoil optimization frameworks; these closed-form expressions may prove particularly useful in gradient-based optimization, where analytical derivatives of the design parameters with respect to the input variables can now be obtained directly.

A. Derivation of Moment Integrals

A. $I_1^{(m)}$: Region $0 \leq x < r$

From Eq. (23),

$$I_1^{(m)} = \int_0^r \left(x^2 - 2rx + 2x_{mc}r - x_{mc}^2 \right) \frac{8x^2 - 6x}{\sqrt{x(1-x)}} \, dx \quad (50)$$

Expanding the polynomial product:

$$\left(x^2 - 2rx + 2x_{mc}r - x_{mc}^2 \right) (8x^2 - 6x) = a_4x^4 + a_3x^3 + a_2x^2 + a_1x \quad (51)$$

with

$$a_4 = 8 \quad (52)$$

$$a_3 = -16r - 6 \quad (53)$$

$$a_2 = 12r + 16x_{mc}r - 8x_{mc}^2 \quad (54)$$

$$a_1 = 6x_{mc}^2 - 12x_{mc}r \quad (55)$$

Applying the substitution $x = \sin^2 \phi$ with $dx/\sqrt{x(1-x)} = 2 d\phi$:

$$I_1^{(m)} = 2 \int_0^{\phi_r} [a_4 \sin^8 \phi + a_3 \sin^6 \phi + a_2 \sin^4 \phi + a_1 \sin^2 \phi] d\phi \quad (56)$$

where $\phi_r \equiv \arcsin(\sqrt{r})$.

Using the reduction formulas:

$$\int \sin^2 \phi d\phi = \frac{\phi}{2} - \frac{\sin \phi \cos \phi}{2} \quad (57)$$

$$\int \sin^4 \phi d\phi = \frac{3\phi}{8} - \frac{3 \sin \phi \cos \phi}{8} - \frac{\sin^3 \phi \cos \phi}{4} \quad (58)$$

$$\int \sin^6 \phi d\phi = \frac{5\phi}{16} - \frac{5 \sin \phi \cos \phi}{16} - \frac{5 \sin^3 \phi \cos \phi}{24} - \frac{\sin^5 \phi \cos \phi}{6} \quad (59)$$

$$\int \sin^8 \phi d\phi = \frac{35\phi}{128} - \frac{35 \sin \phi \cos \phi}{128} - \frac{35 \sin^3 \phi \cos \phi}{192} - \frac{7 \sin^5 \phi \cos \phi}{48} - \frac{\sin^7 \phi \cos \phi}{8} \quad (60)$$

Substituting and grouping:

$$I_1^{(m)} = 2 [A \phi + B \sin \phi \cos \phi + C_3 \sin^3 \phi \cos \phi + C_5 \sin^5 \phi \cos \phi + C_7 \sin^7 \phi \cos \phi]_0^{\phi_r} \quad (61)$$

where

$$A = \frac{35a_4}{128} + \frac{5a_3}{16} + \frac{3a_2}{8} + \frac{a_1}{2} \quad (62)$$

$$B = -A \quad (63)$$

$$C_3 = -\frac{35a_4}{192} - \frac{5a_3}{24} - \frac{a_2}{4} \quad (64)$$

$$C_5 = -\frac{7a_4}{48} - \frac{a_3}{6} \quad (65)$$

$$C_7 = -\frac{a_4}{8} \quad (66)$$

At $\phi = 0$ all terms vanish. At $\phi = \phi_r$, using $\sin \phi_r = \sqrt{r}$ and $\cos \phi_r = \sqrt{1-r}$:

$$I_1^{(m)} = 2A \arcsin(\sqrt{r}) + 2\sqrt{r(1-r)} (B + C_3r + C_5r^2 + C_7r^3) \quad (67)$$

Substituting a_4, a_3, a_2, a_1 and simplifying:

$$2A = \frac{5-8r}{8} \quad (68)$$

$$2(B + C_3r + C_5r^2 + C_7r^3) = \mathcal{P}(r, x_{mc}) \quad (69)$$

where

$$\mathcal{P}(r, x_{mc}) = 4r(x_{mc} - r)^2 + \frac{-16r^3 + 8r^2 + 14r - 15}{24} \quad (70)$$

Therefore:

$$I_1^{(m)} = \frac{5-8r}{8} \arcsin(\sqrt{r}) + \sqrt{r(1-r)} \mathcal{P}(r, x_{mc}) \quad (71)$$

B. $I_2^{(m)}$: Region $r \leq x \leq 1$

From Eq. (24),

$$I_2^{(m)} = \int_r^1 (b_2x^2 + b_1x + b_0) \frac{8x^2 - 6x}{\sqrt{x(1-x)}} dx \quad (72)$$

with b_2, b_1, b_0 as defined in Eqs. (6)–(8).

Expanding the polynomial product:

$$(b_2x^2 + b_1x + b_0)(8x^2 - 6x) = c_4x^4 + c_3x^3 + c_2x^2 + c_1x \quad (73)$$

with

$$c_4 = 8b_2 \quad (74)$$

$$c_3 = -6b_2 + 8b_1 \quad (75)$$

$$c_2 = -6b_1 + 8b_0 \quad (76)$$

$$c_1 = -6b_0 \quad (77)$$

Applying the substitution $x = \sin^2 \phi$:

$$I_2^{(m)} = 2 \int_{\phi_r}^{\pi/2} [c_4 \sin^8 \phi + c_3 \sin^6 \phi + c_2 \sin^4 \phi + c_1 \sin^2 \phi] d\phi \quad (78)$$

Using the same reduction formulas and grouping:

$$I_2^{(m)} = 2 \left[A' \phi + B' \sin \phi \cos \phi + C'_3 \sin^3 \phi \cos \phi + C'_5 \sin^5 \phi \cos \phi + C'_7 \sin^7 \phi \cos \phi \right]_{\phi_r}^{\pi/2} \quad (79)$$

where A', B', C'_3, C'_5, C'_7 follow the same structure as before with c_i replacing a_i .

At $\phi = \pi/2$, all $\sin^{2n+1} \phi \cos \phi$ terms vanish. Using $\frac{\pi}{2} - \phi_r = \arccos(\sqrt{r})$:

$$I_2^{(m)} = 2A' \arccos(\sqrt{r}) - 2\sqrt{r(1-r)} \left(B' + C'_3 r + C'_5 r^2 + C'_7 r^3 \right) \quad (80)$$

Substituting and simplifying:

$$2A' = Q(r, x_{mc}) \quad (81)$$

$$2 \left(B' + C'_3 r + C'_5 r^2 + C'_7 r^3 \right) = R(r, x_{mc}) \quad (82)$$

where

$$Q(r, x_{mc}) = \frac{8r-5}{8} \left[r^3 - 3(x_{mc} - r)^2 \right] \quad (83)$$

$$R(r, x_{mc}) = \frac{r^3}{24} (16r^3 - 8r^2 - 14r + 15) - \frac{1}{8} (32r^4 - 80r^3 + 88r^2 - 46r + 15) (x_{mc} - r)^2 \quad (84)$$

Therefore:

$$I_2^{(m)} = Q(r, x_{mc}) \arccos(\sqrt{r}) - \sqrt{r(1-r)} R(r, x_{mc}) \quad (85)$$

B. Derivation of Lift Integrals

A. $I_1^{(l)}$: Region $0 \leq x < r$

From Eq. (28),

$$I_1^{(l)} = \int_0^r \left(x^2 - 2rx + 2x_{mc}r - x_{mc}^2 \right) \frac{1-2x}{\sqrt{x(1-x)}} dx \quad (86)$$

Expanding the polynomial product:

$$\left(x^2 - 2rx + 2x_{mc}r - x_{mc}^2 \right) (1-2x) = a_3 x^3 + a_2 x^2 + a_1 x + a_0 \quad (87)$$

with

$$a_3 = -2 \quad (88)$$

$$a_2 = 1 + 4r \quad (89)$$

$$a_1 = -2r - 4x_{mc}r + 2x_{mc}^2 \quad (90)$$

$$a_0 = 2x_{mc}r - x_{mc}^2 \quad (91)$$

Applying the substitution $x = \sin^2 \phi$ with $dx/\sqrt{x(1-x)} = 2 d\phi$:

$$I_1^{(l)} = 2 \int_0^{\phi_r} [a_3 \sin^6 \phi + a_2 \sin^4 \phi + a_1 \sin^2 \phi + a_0] d\phi \quad (92)$$

where $\phi_r \equiv \arcsin(\sqrt{r})$.

Using the reduction formulas:

$$\int 1 d\phi = \phi \quad (93)$$

$$\int \sin^2 \phi d\phi = \frac{\phi}{2} - \frac{\sin \phi \cos \phi}{2} \quad (94)$$

$$\int \sin^4 \phi d\phi = \frac{3\phi}{8} - \frac{3 \sin \phi \cos \phi}{8} - \frac{\sin^3 \phi \cos \phi}{4} \quad (95)$$

$$\int \sin^6 \phi d\phi = \frac{5\phi}{16} - \frac{5 \sin \phi \cos \phi}{16} - \frac{5 \sin^3 \phi \cos \phi}{24} - \frac{\sin^5 \phi \cos \phi}{6} \quad (96)$$

Substituting and grouping:

$$I_1^{(l)} = 2 [A \phi + B \sin \phi \cos \phi + C_3 \sin^3 \phi \cos \phi + C_5 \sin^5 \phi \cos \phi]_0^{\phi_r} \quad (97)$$

where

$$A = \frac{5a_3}{16} + \frac{3a_2}{8} + \frac{a_1}{2} + a_0 \quad (98)$$

$$B = -\frac{5a_3}{16} - \frac{3a_2}{8} - \frac{a_1}{2} \quad (99)$$

$$C_3 = -\frac{5a_3}{24} - \frac{a_2}{4} \quad (100)$$

$$C_5 = -\frac{a_3}{6} \quad (101)$$

At $\phi = 0$ all terms vanish. At $\phi = \phi_r$, using $\sin \phi_r = \sqrt{r}$ and $\cos \phi_r = \sqrt{1-r}$:

$$I_1^{(I)} = 2A \arcsin(\sqrt{r}) + 2\sqrt{r(1-r)} (B + C_3r + C_5r^2) \quad (102)$$

Substituting a_3, a_2, a_1, a_0 and simplifying:

$$2A = r - \frac{1}{2} \quad (103)$$

$$2(B + C_3r + C_5r^2) = \mathcal{S}(r, x_{mc}) \quad (104)$$

where

$$\mathcal{S}(r, x_{mc}) = \frac{1}{3} + \frac{2}{3} \left(r - \frac{1}{2} \right)^2 - 2(x_{mc} - r)^2 \quad (105)$$

Therefore:

$$I_1^{(I)} = \left(r - \frac{1}{2} \right) \arcsin(\sqrt{r}) + \sqrt{r(1-r)} \mathcal{S}(r, x_{mc}) \quad (106)$$

B. $I_2^{(I)}$: Region $r \leq x \leq 1$

From Eq. (29),

$$I_2^{(I)} = \int_r^1 (b_2x^2 + b_1x + b_0) \frac{1-2x}{\sqrt{x(1-x)}} dx \quad (107)$$

with b_2, b_1, b_0 as defined in Eqs. (6)–(8).

Expanding the polynomial product:

$$(b_2x^2 + b_1x + b_0)(1-2x) = c_3x^3 + c_2x^2 + c_1x + c_0 \quad (108)$$

with

$$c_3 = -2b_2 \quad (109)$$

$$c_2 = b_2 - 2b_1 \quad (110)$$

$$c_1 = b_1 - 2b_0 \quad (111)$$

$$c_0 = b_0 \quad (112)$$

Applying the substitution $x = \sin^2 \phi$:

$$I_2^{(I)} = 2 \int_{\phi_r}^{\pi/2} [c_3 \sin^6 \phi + c_2 \sin^4 \phi + c_1 \sin^2 \phi + c_0] d\phi \quad (113)$$

Using the same reduction formulas and grouping:

$$I_2^{(I)} = 2 \left[A' \phi + B' \sin \phi \cos \phi + C'_3 \sin^3 \phi \cos \phi + C'_5 \sin^5 \phi \cos \phi \right]_{\phi_r}^{\pi/2} \quad (114)$$

where A', B', C'_3, C'_5 follow the same structure as before with c_i replacing a_i .

At $\phi = \pi/2$, all $\sin^{2n+1} \phi \cos \phi$ terms vanish. Using $\frac{\pi}{2} - \phi_r = \arccos(\sqrt{r})$:

$$I_2^{(I)} = 2A' \arccos(\sqrt{r}) - 2\sqrt{r(1-r)} \left(B' + C'_3 r + C'_5 r^2 \right) \quad (115)$$

Substituting and simplifying:

$$2A' = \mathcal{T}(r, x_{mc}) \quad (116)$$

$$2 \left(B' + C'_3 r + C'_5 r^2 \right) = \mathcal{U}(r, x_{mc}) \quad (117)$$

where

$$\mathcal{T}(r, x_{mc}) = \left(\frac{1}{2} - r \right) \left[r^3 - 3(x_{mc} - r)^2 \right] \quad (118)$$

$$\mathcal{U}(r, x_{mc}) = \frac{1}{2} (4r^3 - 8r^2 + 8r - 1)(x_{mc} - r)^2 - \frac{r^3}{6} (4r^2 - 4r + 3) \quad (119)$$

Therefore:

$$I_2^{(I)} = \mathcal{T}(r, x_{mc}) \arccos(\sqrt{r}) - \sqrt{r(1-r)} \mathcal{U}(r, x_{mc}) \quad (120)$$

C. Extended-Precision Breakpoint Values

For reproducibility, Table 11 reports the analytical breakpoint parameter r to eight decimal places for the cases considered in Section V.A. These values satisfy the zero-moment condition to machine precision.

Table 11 Extended-precision breakpoint parameter r for representative reflex configurations.

Designation	x_{mc}	r_{ref}	r_{anal}	$r_{\text{anal}} - r_{\text{ref}}$
221	0.10	0.1300	0.13074976	$+7.4976 \times 10^{-4}$
231	0.15	0.2170	0.21601450	-9.8550×10^{-4}
241	0.20	0.3180	0.31791890	-8.1100×10^{-5}
251	0.25	0.4410	0.44083034	-1.6966×10^{-4}

Funding Sources

No external funding was received for this research.

Acknowledgments

The author gratefully acknowledges the foundational work of Ira H. Abbott and Albert E. von Doenhoff of the National Advisory Committee for Aeronautics, and the historical airfoil-ordinate tabulations compiled by Charles L. Ladson and Cuyler W. Brooks Jr. of NASA Langley Research Center, which provided the essential reference data for validation. AI-assisted tools (Claude and ChatGPT) were used for grammar checking, code assistance, and manuscript formatting; the author assumes full responsibility for the technical content and has verified all results independently.

References

- [1] Abbott, I. H., and von Doenhoff, A. E., *Theory of Wing Sections: Including a Summary of Airfoil Data*, Dover Publications, New York, 1959.
- [2] Jacobs, E. N., and Pinkerton, R. M., "Tests in the Variable-Density Wind Tunnel of Related Airfoils Having the Maximum Camber Unusually Far Forward," NACA Report 537, National Advisory Committee for Aeronautics, 1935.
- [3] Ladson, C. L., and Brooks, J., C. W., "Development of a Computer Program To Obtain Ordinates for NACA 4-Digit, 4-Digit Modified, 5-Digit, and 16-Series Airfoils," NASA Technical Memorandum TM-3284, National Aeronautics and Space Administration, Nov. 1975.
- [4] Glauert, H., *The Elements of Aerofoil and Airscrew Theory*, Cambridge University Press, Cambridge, UK, 1926.